Molecularly Imprinted Mesoporous Organosilica

Jennifer E. Lofgreen,[†] Igor L. Moudrakovski,[‡] and Geoffrey A. Ozin[†,*]

[†]Department of Chemistry, University of Toronto, Toronto, Ontario M6S 3H6, Canada and [‡]Steacie Institute for Molecular Sciences, National Research Council Canada, Ottawa, Ontario K1A 0R6, Canada

ABSTRACT We have prepared molecularly imprinted mesoporous organosilica (MIMO) using a semicovalent imprinting technique. A thermally reversible covalent bond was used to link a bisphenol A (BPA) imprint molecule to a functional alkoxysilane monomer at two points to generate a covalently bound imprint precursor. This precursor was incorporated into a cross-linked periodic mesoporous silica matrix *via* a typical acid-catalyzed, triblock copolymer-templated, sol−gel synthesis. Evidence of imprint sites buried in the pore walls was found through careful characterization of the imprinted material and its comparison to similarly prepared non-imprinted mesoporous organosilica (NIMO) and pure periodic mesoporous silica (PMS). After thermal treatment, the imprinted material (MIMO-ir) removed more than 90% of appropriately sized bisphenol species from water, yet showed significantly lower binding for both smaller and larger molecules containing phenol moieties. Identically treated NIMO-ir showed much poorer retention behavior than MIMO-ir for the same bisphenol species and behaved only slightly better than PMS-ir.

KEYWORDS: molecular imprint · periodic mesoporous organosilica · solid-phase extraction · bisphenol A · hybrid material

Molecular imprinting can be defined as the assembly of a cross-linked polymer matrix around an imprint molecule that is held in place, either covalently or noncovalently, by judiciously chosen functional monomers. The removal of the imprint molecule yields an imprint cavity of a specific size. The surface of the imprint cavity contains functional groups that are able to interact, either covalently or noncovalently, with certain moieties on an appropriately sized target molecule. This concept was first demonstrated in silica in 1931,[1] yet the majority of the literature to date is focused on molecular imprinting in organic polymers;[2] it is only in the past decade that interest in molecular imprinting in silica has seen a revival.[3−5] This could be due to a major difference in the swellability of commonly used organic polymers compared to silica. While organic polymers can easily be customized to swell and shrink by controlled amounts in response to stimuli such as solvent exposure and applied voltage,[6] silica is more rigid, and this can cause a problem for molecular imprinting. Slow diffusion through bulk silica can severely hamper access to imprint sites,[7] which could be why the molecular imprinting community first abandoned silica as a matrix. A simple way to overcome this diffusion problem is to reduce the diffusion distance. Several reports of molecular imprinting in thin films of silica have confirmed that significantly improved target interaction can be achieved by reducing the diffusion length.[4,8−10] Alternatively, surface imprinting on silica eliminates the need for diffusion altogether,[11,12] but in the case of organic molecules, this method does risk sacrificing the size and shape selectivity that can be achieved by creating a closed imprint cavity.

Thin films may be useful for sensing and other analytical applications, but if molecularly imprinted silica is to be used for preparative applications or produced in larger quantities for industrial use, a better choice of morphology is silica powder; it can easily be packed into columns or other vessels, suspended in various solvents and then isolated by centrifugation or filtration, and washed and dried for reuse. In this case, the way to overcome the diffusion problem is to make the silica powder highly porous. Specifically, the solution is to create a close-packed network of nanometer-sized channels in the silica matrix, thereby reducing the diffusion distance to the order of a few nanometers. The choice of channels instead of closed pores increases the likelihood that they will be open at the outer surface of individual particles, thus further reducing the amount of silica through which a molecule must diffuse to reach an imprint site and allowing for easier flow through the material.

This type of porosity is easily created using a sol−gel approach involving a micelle template in aqueous media, to generate a mesoporous material. Two common

* Address correspondence to gozin@chem.utoronto.ca.

Received for review December 22, 2010 and accepted February 7, 2011.

Published online February 16, 2011
10.1021/nn1035697

© 2011 American Chemical Society

periodic mesoporous silicas (PMSs), MCM-41[13] and SBA-15,[14] prepared using an alkoxysilane sol−gel precursor with ionic surfactant and nonionic copolymer templates, respectively, have the same hexagonal close-packed channel pore structure but differ in surface area, pore diameter, and wall thickness. Periodic mesoporous organosilica (PMO) can be prepared in exactly the same way as PMS but has bridging organic groups covalently bound to at least two silicon atoms each in the silica matrix. Organosilica can refer to any silica-based material that contains silicon−carbon covalent bonds. We report herein the synthesis, characterization, and utility of a molecularly imprinted mesoporous organosilica (MIMO). Reports on ionic and molecular imprinting in MCM-41 have shown good target response,[15,16] yet to our knowledge, there has not yet been reported a thorough study of the mesoporous material itself at all stages of the material synthesis to state with confidence the actual location of imprint sites in the material and the preservation of the material's morphology (particularly the mesostructure) throughout. We believe this is essential to proving successful molecular imprinting *in* (not *on*) mesoporous materials, as most large silane-functionalized organic moieties are very difficult to incorporate into the pore walls of micelle-templated mesoporous silica, preferring instead to occupy surface sites or extend into the pores. For this study, a covalently bound imprint molecule was incorporated into SBA-15-type mesoporous silica, as it possesses larger pore diameters, thicker walls, and better hydrothermal stability than MCM-41. This provides both better access to imprint sites through wider channels and a more robust silica matrix due to thicker pore walls that are better able to maintain the shape of the imprint cavity compared to MCM-41, while still offering the necessary high surface area and short diffusion distances for better access to imprint sites than in bulk silica. The chosen imprint molecule was bisphenol A (BPA), a well-known endocrine disruptor that has received significant attention in recent years due to concern over its presence in a variety of consumer products including food packaging, food storage containers, and baby bottles.[17] BPA is not only a relevant choice of imprint; it comes from a large family of phenol-containing molecules, the bisphenols, which offers the opportunity for a systematic study of the relationship between small, stepwise changes in structure and a BPA-imprinted material's response to the corresponding target molecule.

In order to create a well-defined imprint site yet achieve rapid target molecule interaction, a semicovalent imprinting approach was used.[18] The imprint was covalently bound to the functional monomers through a thermally reversible carbamate bond that was formed by a direct coupling between phenol moieties on BPA and isocynanate groups on (3-isocyanatopropyl)triethoxysilane

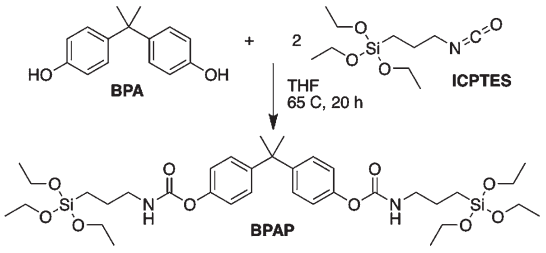

Scheme 1. Synthesis of BPAP by a direct coupling reaction between stoichiometric amounts of phenol on BPA and isocyanate on ICPTES.

(ICPTES) (Scheme 1). The precursor, BPAP, was produced nearly quantitiatively (90% by NMR) from the reaction of a 1:2 stoichiometric mixture of BPA and ICPTES. This direct coupling reaction uses no catalysts or co-reactants and requires only a solvent evaporation step to isolate the product. It is a simple synthetic method that is highly amenable to scale-up.

Molecularly imprinted periodic mesoporous organosilica (MIMO) powder was prepared by a triblock-copolymer-templated sol−gel method (Scheme 2). A solution of 10 mol % Si from BPAP in 90 mol % Si from tetraethyl orthosilicate (TEOS) was prepared and completely dissolved to ensure uniform distribution of BPAP throughout the TEOS cross-linker. This solution was added to a solution of Pluronic P123 ($PEO_{20}PPO_{70}$-PEO_{20}) and NaCl in aqueous HCl with a Si:HCl:P123:H_2O:NaCl molar ratio of 1:6.13:0.022:228:0.006. A non-imprinted periodic mesoporous organosilica (NIMO) with a terminal organic group instead of a bridging one was similarly prepared using the same molar amount of Si from ICPTES in place of BPAP. A control periodic mesoporous silica (PMS) was also prepared by the same method using only TEOS. In order to cleave the carbamate bonds in MIMO and produce the final imprinted material, MIMO-ir, a portion of the powder was suspended in wet dimethylsulfoxide (DMSO) and stirred at 160 °C. Identical treatments were done on NIMO and PMS samples, yielding NIMO-ir and PMS-ir, respectively.

RESULTS AND DISCUSSION

In order to state that MIMO does indeed contain molecular imprint sites and that MIMO-ir does indeed function as an effective molecularly imprinted mesoporous organosilica material, simple rebinding tests alone are not sufficient. An inherent challenge in the generation of a new PMO species is the limitation of the types of organic bridging groups that can be used. It is generally accepted that large flexible organic bridging groups are difficult, if not impossible, to incorporate into the pore walls of a PMO, as they either disrupt the self-assembly to such a degree that a disordered or nonporous material is produced, phase separate to yield a mixture of dense organosilica and PMS, or interact with the pore template and reside on the pore surfaces instead of within the pore

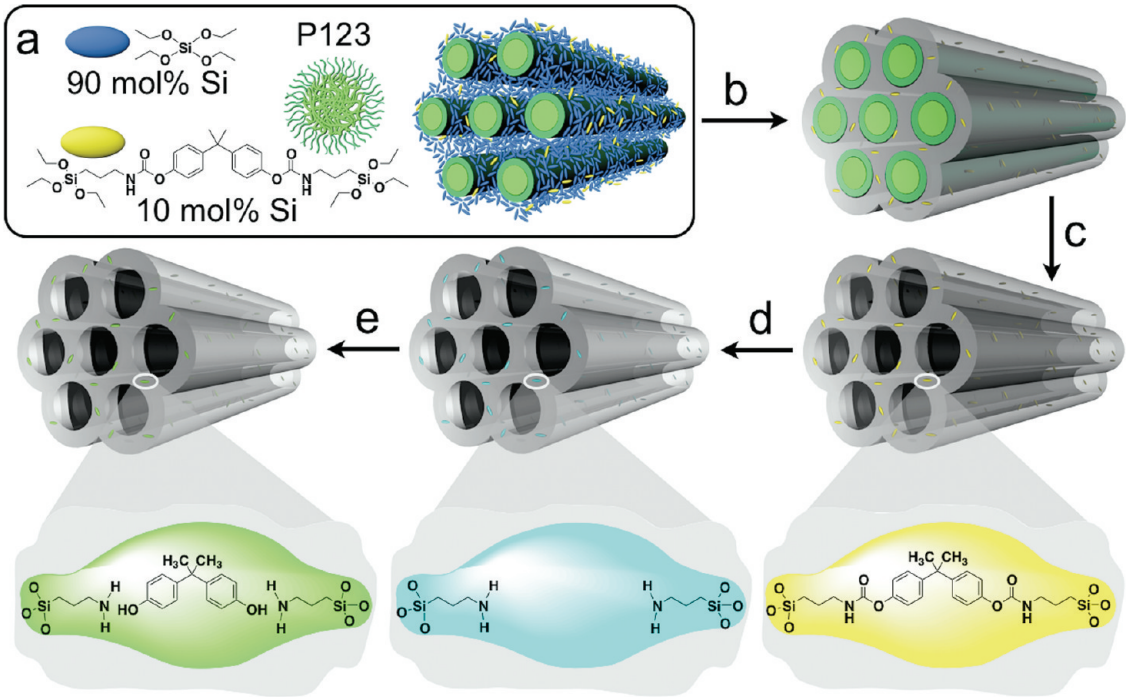

Scheme 2. Synthesis of molecularly imprinted mesoporous organosilica (MIMO), imprint removal to yield MIMO-ir, and interaction of a target molecule with the imprint site: (a) the mixture of TEOS and BPAP assembles around and between the hexagonal close-packed core−shell micelles of P123 in acidic aqueous media; (b) stirring at room temperature for 24 h followed by quiescent curing at 80 °C for 24 h; (c) P123 template removal by Soxhlet extraction with ethanol for 20 h; (d) thermal cleavage of the imprint by heating in wet DMSO for 5 h; (e) sequestration of an appropriately sized target bisphenol molecule by hydrogen bonding between phenols and amines.

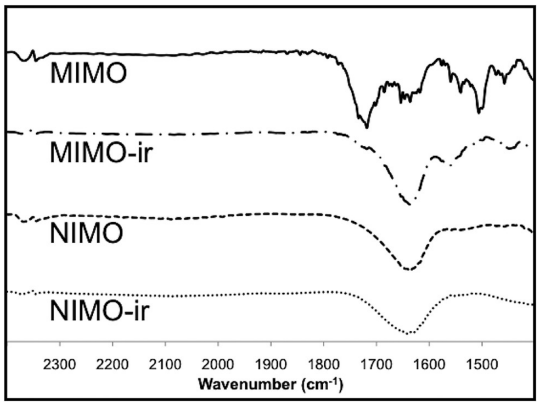

Figure 1. Fourier transform infrared spectra of MIMO (solid trace), MIMO-ir (dot-dashed trace), NIMO (dashed trace), and NIMO-ir (dotted trace).

walls. Even if a given PMO is successfully synthesized, it is difficult to state unequivocally the location of the organic bridging groups. Thus, the introduction of a new organosilica precursor of the size used here carries with it the concern that one of the above three situations will arise during the material synthesis, and careful examination of MIMO and its comparison to NIMO and PMS (and their thermally treated counterparts) is therefore of the utmost importance. This comparison relies on a combination of common characterization techniques for periodic mesoporous materials and the behavior of MIMO-ir, NIMO-ir, and PMS-ir in size- and shape-selective target rebinding studies.

In order to ensure a valid comparison, significant care was taken to control the distinctions between the three materials, from the molar ratios of the different precursors in the material synthesis to the postsynthetic treatment steps. This was necessary to reduce the number of variables in the system, and consequently, the chemical composition, organic loading, pore structure, and physicochemical properties were carefully determined for all materials at each step. Rebinding tests were not performed until all parameters were evaluated and a satisfactory and controllable degree of variation between materials was demonstrated.

Chemical Composition of the Materials. To confirm the successful cleavage of the carbamate bond in MIMO-ir, the solid materials were characterized by Fourier transform infrared spectroscopy (Figure 1). The carbamate C═O stretch at 1720 cm^{-1} is clearly visible for the as-synthesized MIMO sample (solid trace) and is eliminated after thermal treatment (dashed trace). No isocyanate (NCO) stretch appears at 2270 cm^{-1} in the MIMO-ir spectrum, showing that the thermal bond cleavage does not regenerate the original NCO group and indicating that the carbamate is indeed converted to a primary amine. The NH_2 bending mode at about 1670 cm^{-1} overlaps with an OH bending mode at 1640 cm^{-1}, but it can still be identified by the asymmetry of the peak. NIMO shows no isocyanate stretch, indicating that the NCO group was converted to an amine during heating in the presence of water and acid in the synthesis solution.

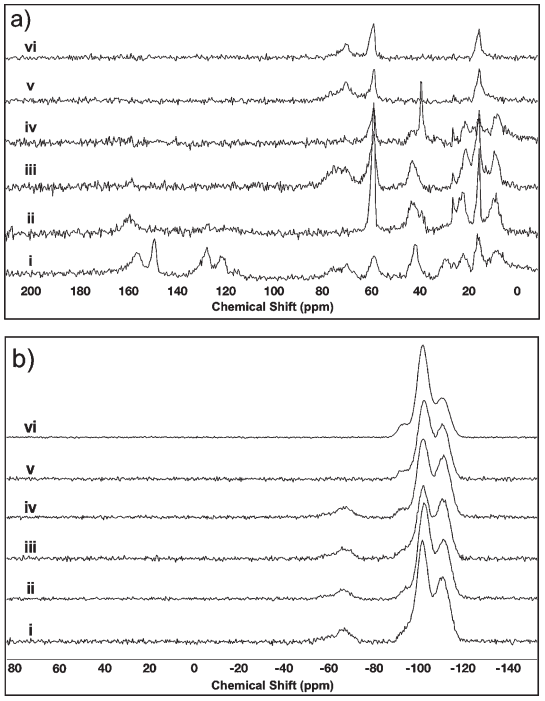

Figure 2. (a) ^{13}C CP MAS spectra and (b) ^{29}Si CP MAS spectra of (i) MIMO, (ii) MIMO-ir, (iii) NIMO, (iv) NIMO-ir, (v) PMS, and (vi) PMs-ir.

The asymmetric peak at 1640 cm^{-1} can again be assigned to overlapping NH_2 bending and OH bending in silica. NIMO-ir shows no difference, which was anticipated as no further chemical modifications were expected to occur for this sample (for full spectra of all samples, see Supporting Information).

To obtain a more comprehensive characterization of the composition of the materials, solid-state nuclear magnetic resonance (SSNMR) spectroscopy was employed. ^{13}C cross-polarized magic-angle spinning (CP MAS) spectra (Figure 2a) were obtained for all samples to confirm the presence of the expected organic groups. In the MIMO spectrum (trace i), the aromatic carbons (120−160 ppm) and the methyl carbons (30 ppm) of the BPA imprint are clearly present, as well as the anchoring propyl groups (8, 22, and 42 ppm). Residual ethoxy moieties (16 and 58 ppm) and some residual P123 template (70−80 ppm) are also present. P123 is eliminated after thermal treatment, likely due to the extra washing of the material. The aromatic and methyl carbon peaks also disappear into the baseline after thermal treatment, while the relative intensity of the carbon signals in the remaining aminopropyl (AP) groups is unchanged, indicating that most of the imprint molecules were removed without affecting the anchoring groups. A slight peak at 39.5 ppm indicates the presence of some residual DMSO from the thermal treatment, and residual ethoxy groups are also still present. In the NIMO spectrum (trace iii), the propyl carbons of the AP groups are clearly present, as are some residual P123 and surface ethoxy groups. The

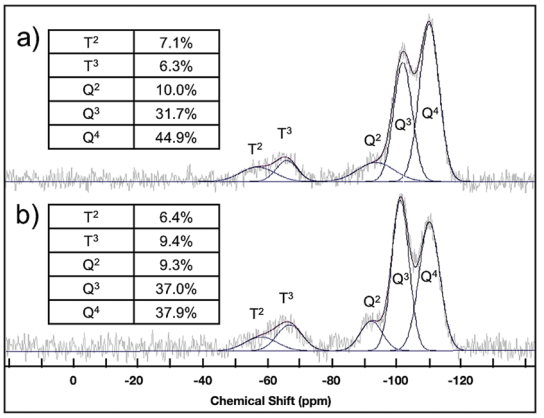

Figure 3. ^{29}Si HPDEC spectra of (a) MIMO-ir and (b) NIMO-ir (gray traces) and fitting (black traces) showing individual Gaussian peaks. Insets: integration of the individual Gaussian peaks for each plot and the corresponding Si species.

P123 signals disappear after thermal treatment (trace iv), while a residual DMSO peak appears and the AP and ethoxy carbon signals persist. As expected for PMS (trace v), the only carbon signals are those of residual ethoxy groups and a small amount of P123, which after thermal treatment (trace vi) remain unaffected. These data confirm that MIMO-ir and NIMO-ir contain the same carbon species and therefore the same AP groups, which makes a comparison of their performance in bisphenol extraction valid. Conversely, PMS-ir contains only residual ethoxy carbon species, making it possible to use this sample to determine how the unmodified mesoporous silica matrix interacts with the chosen analytes.

^{29}Si CP MAS spectra were taken of all samples to identify the silicon species present in each material (Figure 2b). For MIMO (trace i), MIMO-ir (trace ii), NIMO (trace iii), and NIMO-ir (trace iv), five ^{29}Si species can be identified. Two T species, T^2 ($RSiO_2OR'$, −52 ppm) and T^3 ($RSiO_3$, −65 ppm), correspond to the $RSiO_xOR'_{3-x}$ sites containing the AP functional groups (R = BPAP organic bridge or AP anchor; see Scheme 2, R′ = OH or OCH_2CH_3), while the remainder of the matrix is composed of Q sites, $SiO_xOR'_{4-x}$, namely, Q^2 ($SiO_2(OR')_2$, −92 ppm), Q^3 (SiO_3OR',-102 ppm), and Q^4 (SiO_4, −110 ppm). As expected, PMS (trace v) and PMS-ir (trace vi) show only Q species.

Quantification of the Imprint Sites. In order to quantify the number of T sites and to estimate the number of imprint sites or non-imprinted amine groups in the MIMO-ir and NIMO-ir materials, respectively, quantitative ^{29}Si high-power decoupling (HPDEC) MAS spectra were taken of these two samples (Figure 3). The peak positions of the different Si species in these samples were determined by fitting Gaussian peaks to the ^{29}Si CP MAS spectra; these positions were subsequently used to fit the HPDEC MAS spectra with Gaussian peaks that were then integrated.[19] Both MIMO-ir and NIMO-ir had a higher

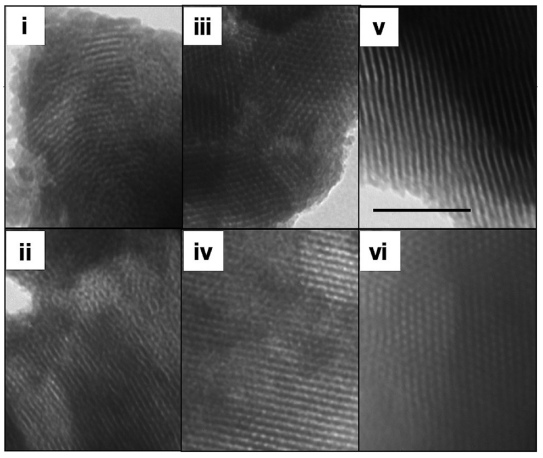

Figure 4. TEM images of (i) MIMO, (ii) MIMO-ir, (iii) NIMO, (iv) NIMO-ir, (v) PMS, and (vi) PMS-ir. All images are shown to the same scale. Scale bar = 100 nm.

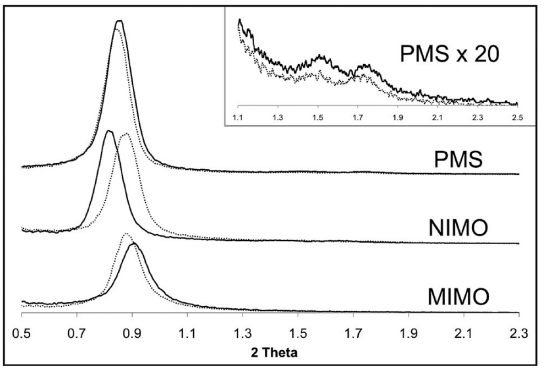

Figure 5. X-ray diffraction plots for MIMO, NIMO, and PMS (solid traces) and MIMO-ir, NIMO-ir, and PMA-ir (dotted traces) showing the (100) peak. All plots are to the same scale. Inset: enlargement of second-order (110) and (200) diffraction peaks for PMS (solid) and PMS-ir (dotted).

proportion of T species than expected from the original synthesis conditions (13.4 and 15.8%, respectively, compared to 10% in the original synthetic mixture). While a small fraction of this discrepancy may have arisen from the peak fitting, a more likely reason is that the hydrolysis and polycondensation (or gelation) rates of $(R'O)_3SiRSi(OR')_3$-type silanes, where the bridging R is long and flexible (as with BPAP), are known to be faster than those of TEOS.[20] It is therefore likely that less BPAP would remain unreacted than TEOS, some of which which would be more likely to remain in solution. However, these results are still below the established 25 mol % threshold for the successful incorporation of nonrigid or terminal organic groups into a mesoporous silica material that does not collapse upon removal of the template.[21] This indicates that the AP sites are likely to be homogeneously distributed throughout the materials, and that the imprint sites are likely buried in the pore walls, not dangling on the internal pore or external particle surfaces. The low loading of imprint sites was designed with this in mind, in order to reduce the possibility that the overall mesopore structure would collapse following thermal removal of the imprint molecules, as this step effectively breaks cross-links in the material.

From the fraction of T species, the number of imprint sites in MIMO-ir and non-imprinted amine sites in NIMO-ir were determined. MIMO-ir and NIMO-ir contain exactly the same functional groups, so their empirical formulas can be directly compared. MIMO-ir contains 13.4 mol % T, which yields an approximate empirical formula of $SiO_{1.93}(CH_2CH_2CH_2NH_2)_{0.13}$. Each imprint site contains two T species, so for every gram of MIMO-ir, there are 2.0×10^{-3} mol AP groups, or 1.0×10^{-3} mol imprint sites. NIMO-ir contains 15.8 mol % T, so its empirical formula is $SiO_{1.92}(CH_2CH_2CH_2NH_2)_{0.16}$. For every gram of NIMO-ir, there are 2.3×10^{-3} mol AP groups, or the equivalent of $1.1(5) \times 10^{-3}$ mol "imprint" sites or pairs of AP groups. In other words, NIMO-ir has approximately 15% more AP groups than MIMO-ir per gram of material.

Effect of the Organic Groups on the Pore Structure. The preservation of the mesoporous structure was confirmed visually by transmission electron microscopy (TEM) of all three materials before and after thermal treatment (Figure 4). There is no discernible difference in pore structure or size in any of the materials before and after the imprint removal treatment. However, there is a clear difference in the long-range order of the mesopores going from MIMO to NIMO to PMS: PMS/PMS-ir show long-range ordering both perpendicular and parallel to the channels; NIMO/NIMO-ir show good ordering and parallel channels, but the domains are noticeably smaller; MIMO/MIMO-ir show relatively parallel channels and some evidence of a hexagonal pore structure, but the pores are significantly more disordered. This trend is also evident in the small-angle X-ray diffraction (XRD) data obtained for each of the samples (Figure 5). The broadest and least intense (100) reflections were obtained for MIMO and MIMO-ir; those of NIMO and NIMO-ir are slightly sharper and more intense. Only PMS and PMS-ir exhibit any higher order diffraction peaks ((110) and (200)). The large two-point-attached imprint precursor, BPAP, was expected to have a somewhat disruptive effect on the self-assembly of the P123 in solution, so it is logical that MIMO and MIMO-ir show the poorest pore ordering. (3-Aminopropyl)triethoxysilane (APTES) has been shown to have a significantly disruptive effect on the structural ordering of SBA-15 when synthesized in acidic media due to the protonation of the amines.[22] However, this effect was not as pronounced in the synthesis of NIMO since the AP groups were produced by the reduction of NCO groups; amine groups were not introduced in significant amounts until after the micelle self-assembly and intitial condensation of the silica matrix had occurred. As such, a small amount of disorder due to the incorporation of nonrigid ICPTES can be expected, which accounts for the moderate ordering observed in

TABLE 1. Physicochemical Properties of the Prepared Mesoporous Materials Determined from Nitrogen Adsorption and X-ray Diffraction

sample	BET surface area (m^2/g)	pore diameter (nm)	pore volume (cm^3/g)	d(100) (nm)	wall thickness[a] (nm)
(i) MIMO	552	5.81	0.66	9.7	5.4
(ii) MIMO-ir	398	6.72	0.49	10.0	4.9
(iii) NIMO	629	8.06	0.92	10.8	4.4
(iv) NIMO-ir	552	6.75	0.66	10.0	4.8
(v) PMS	594	6.71	0.69	10.3	5.2
(vi) PMS-ir	661	6.74	0.66	10.5	5.3

[a] Calculated by thickness = $2 \times d(100)/\sqrt{3}$ − pore diameter.

NIMO and NIMO-ir. The best ordering is observed for PMS and PMS-ir because TEOS facilitates micelle self-assembly[23] and is known to yield excellent long-range ordering when used to prepare P123-templated PMS.[14]

Determining the Location of the Imprint Sites. Nitrogen gas adsorption was performed on each material to determine surface area, pore size, and pore volume. All materials exhibited type IV isotherms with H1 hysteresis typical of SBA-15-type mesoporous materials containing ordered cylindrical pores (Supporting Information).[14,24] The pore diameter was found by BJH theory using the adsorption branch of each isotherm and was used along with the *d*-spacing found from XRD to calculate the pore wall thickness (Table 1). The surface areas, pore diameters, and pore volumes of all materials fall within the expected range for this class of material, yet there are noticeable differences in the precise values. NIMO displays a slightly larger than typical pore diameter and a smaller wall thickness. This suggests that the ICPTES was mostly localized at the micelle surface during the material synthesis, causing swelling of the template, which resulted in an expanded pore structure with the AP groups on the pore surface. The pore diameter of MIMO, however, is much more similar to that of PMS, while the pore wall is slightly thicker. This indicates that the BPAP resided between micelles during the material synthesis, causing a slight expansion of the micellar phase but having minimal effect on the templated pore sizes. Thus it is reasonable to conclude that the imprint sites are indeed buried in the walls of MIMO/MIMO-ir and not located on the surface of the pores.

Solid-Phase Extraction and Static Binding Tests. To determine whether MIMO-ir was actually molecularly imprinted, target binding tests were performed using three sets of phenol-containing compounds (Scheme 3). Series 1 contained three targets (BPF, BPA, and BPAF), which have similar size and arrangement of phenol moieties but increasing hydrophobicity due to substitution at the bridging carbon atom (indicated by an asterisk in Scheme 3, series 1); series 2 contained four targets (P, R, BP, and BPA), which possess varying numbers and arrangements of phenol groups and aromatic rings; series 3 was a single target (BTB) that possesses the correct number and arrangement of phenol groups but is significantly larger than BPA and has more crowded phenol groups.

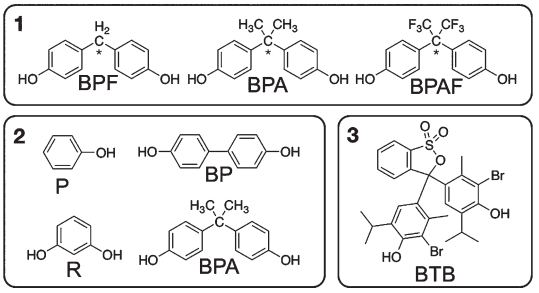

Scheme 3. Compounds used in target binding tests. Series 1: bisphenol F (BPF), bisphenol A (BPA), hexafluorobisphenol A (BPAF). Series 2: phenol (P), resorcinol (R), 4,4′-biphenol (BP), and bisphenol A (BPA). Series 3: bromothymol blue (BTB). Asterisks in series 1 indicate the bridging carbon at which different substitution gives rise to different hydrophobicity in this series.

Solid-phase extraction (SPE) is a useful separation technique that can be used to isolate desired compounds from an impure or mixed solution; as in liquid chromatography, separation is achieved as a result of differences in affinity between compounds in a solution and the stationary phase through which the solution flows. MIMO-ir, NIMO-ir, and PMS-ir were evaluated using a simplified SPE method (Scheme 4). First, a precise amount of powder (MIMO-ir, NIMO-ir, or PMS-ir) was sandwiched between filter paper in a polyethylene syringe to create a simple SPE cartridge. To this cartridge was added 1.0 mL of an aqueous stock solution (either series 1 or series 2). This load volume was allowed to flow through the syringe by gravity and collected in a vial. As soon as the load solution had fully passed into the cartridge, a rinse of 1.0 mL water was added to wash out any weakly adsorbed molecules. As the rinse flowed through, the remainder of the load solution was forced through the cartridge and collected, and in a second vial, the rinse solution was then collected. Once the rinse had flowed into the cartridge, a total of 6.0 mL of acetonitrile (ACN) was used to elute any strongly bound molecules from the cartridge. The remainder of the rinse fraction was forced through by the eluent and collected. Finally, a total of 6.0 mL of

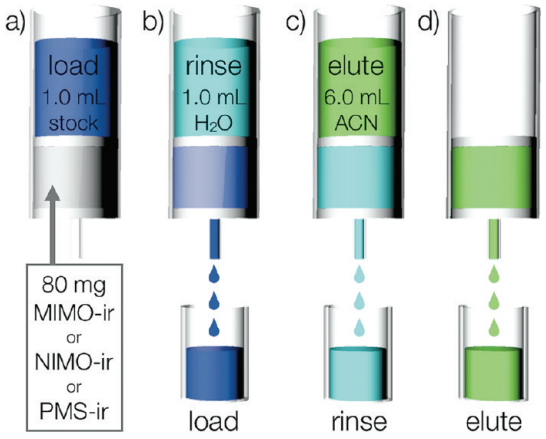

Scheme 4. Solid-phase extraction method employing load, rinse, and elute steps: (a) a syringe packed with powder is loaded with 1.0 mL of stock solution; (b) the load flows through by gravity into a vial; 1.0 mL of rinse water is added immediately following the load, which is collected quantitatively and analyzed; (c) the rinse flows through by gravity into a second vial; 6.0 mL of ACN is added immediately following the rinse, which is collected quantitatively and analyzed; (d) a total of 6.0 mL of ACN is collected in a third vial as the eluent and evaporated to dryness; the residue is redissolved in 1.0 mL ACN and analyzed.

ACN was collected in a third vial. This eluent fraction was evaporated to dryness, and the residue was redissolved in 1.0 mL of ACN. The load, rinse, and redissolved elute fractions were analyzed immediately by HPLC to find the concentration of each analyte and compared to the corresponding stock solution.

In the first test, series 1 was used. As expected for a molecularly imprinted material, MIMO-ir removed most of all three species from series 1 (Figure 6a). Greatest retention was observed for the most hydrophobic analyte, BPAF, followed by the smallest analyte, BPF, with the smallest retention observed for the imprint molecule, BPA; overall, however, all three targets were more than 85% retained after the load and rinse steps. This can be explained by considering that the most favorable binding is for the most hydrophobic analyte, and that the smallest analyte would most easily diffuse into the imprint site. Being non-imprinted, NIMO-ir and PMS-ir showed an interesting and logical trend: BPF, the least hydrophobic molecule, was the least retained, and BPAF, the most hydrophobic, was the most retained; in fact, more BPAF was retained after loading in NIMO-ir than BPA was retained in MIMO-ir. NIMO-ir retained approximately 5% more of each analyte than did PMS-ir after loading, suggesting that silica alone does have some ability to retain bisphenol species in solid-phase extraction from aqueous solution, and that only a small enhancement of this retention is achieved through the incorporation of 15% AP groups. Rinsing was sufficient to recover more than 80% of BPF and BPA from NIMO-ir and PMS-ir, indicating that the major contributor to their moderate retention is weak interactions with surface functional groups on the mesoporous materials. BPAF

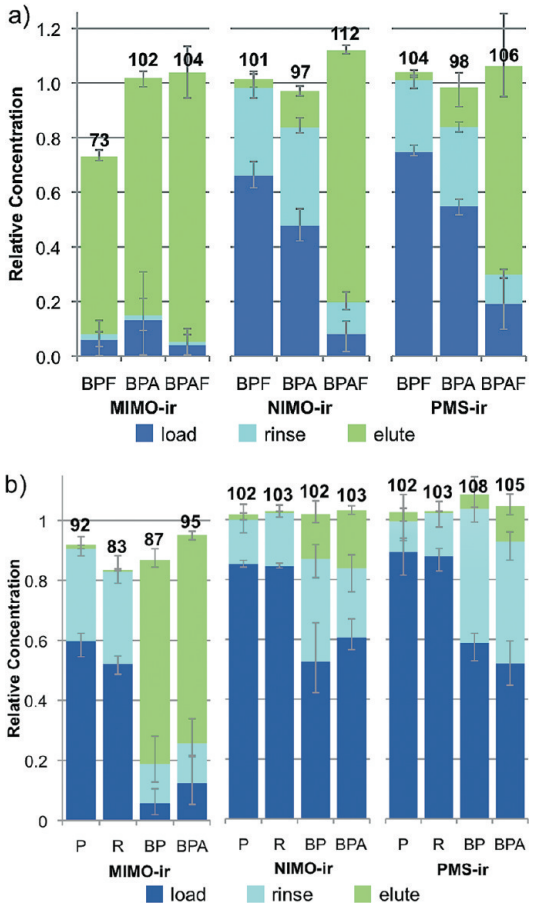

Figure 6. (a) Stacked solid-phase extraction plots for series 1: the concentration of BPF, BPA, and BPAF relative to an aqueous stock solution of BPF, BPA, and BPAF, each at a concentration of 1×10^{-4} M. (b) stacked solid-phase extraction plots for series 2: the concentration of P, R, BP, and BPA relative to an aqueous stock solution of P, R, BP, and BPA, each at a concentration of 1×10^{-4} M. Numbers at the top of each column indicate the total percent of each target recovered.

was more strongly retained in both NIMO-ir and PMS-ir, which is likely due to its significantly larger hydrophobic character. Rinsing with water, a poor solvent for BPAF, does little to disrupt the weak interactions between BPAF and the (organo)silica matrix to which it is adsorbed.

In series 2, which contained P, R, BP, and BPA, the importance of the arrangement and spacing of phenol groups for binding is clearly demonstrated (Figure 6b). Although P and R are very small molecules and possess the appropriate functional groups, they were poorly retained in MIMO-ir. BP and BPA, on the other hand, were retained very well; BP was better retained than BPA, which can again be explained by its smaller size and greater ease of diffusion into the imprint sites. NIMO-ir and PMS-ir displayed very similar retention behavior for series 2, with the general trend corresponding approximately to the hydrophilic/hydrophobic nature of the targets. The retention behavior of MIMO-ir for smaller molecules than the imprint is encouraging: higher retention than NIMO-ir suggests

that there are indeed imprint cavities in the material which are able to trap some molecules as they flow through the SPE cartridge, yet low retention after rinsing confirms that good binding can only be achieved when the target is of a large enough size that two-point binding within the imprint site is possible.

Solid-phase extraction relies on rapid interaction between the solid-phase material and the target molecule. A concern with the use of mesoporous materials was that most of the load solution would pass around the MIMO-ir particles instead of entering the mesopore channels, thus negating the imprinting altogether. If this was the case, it was expected that MIMO-ir and PMS-ir would show similar behavior in retention of the targets in series 1 and 2 since the outer surfaces of particles of these two materials are similar: since the imprint sites are mostly buried within the pore walls of MIMO-ir, the outer surface of MIMO-ir particles contains almost no organic functional groups, and as such it very closely resembles unmodified silica. The few imprint sites that may exist on the outer surface of MIMO-ir particles can only account for a tiny difference from PMS-ir in retention behavior. However, as a significant difference was observed in the extraction properties of MIMO-ir and PMS-ir, it is possible to conclude that the load solution is indeed penetrating into the mesopores of the materials and, therefore, able to access imprint sites buried in the walls. Likewise, if the binding were simply due to interactions with amine groups on the surface of the pores or the outer surfaces of the particles, it was expected that NIMO-ir would show better binding than MIMO-ir, due to its larger concentration of AP groups and the localization of these groups on the pore walls. This, too, was not the case, indicating conclusively that, although buried in the pore walls, the imprint sites are accessible to aqueous solutions. Additionally, binding in the imprint site must occur rapidly since the load solutions were flowed through each cartridge by gravity in five minutes or less. If binding were slow, only very low flow rates would yield good extraction. Overall, it is clear that for the removal of bisphenol species from water that the addition of AP groups alone to silica is not sufficient; in other words, the arrangement and spacing of these groups, achieved in this case by molecular imprinting, are necessary to achieve good sequestration.

To confirm that a size-selective imprint cavity had been created in MIMO-ir, an aqueous solution of bromothymol blue (BTB, Scheme 3) was used. The number and arrangement of phenols in BTB is similar to BPA (Scheme 3, series 3), so similar binding for these two molecules should be observed if the imprint sites are either not buried in the walls or are not size-selective. Qualitatively, the solutions suspended with PMS-ir (2) and MIMO-ir (3) still retain most of their color

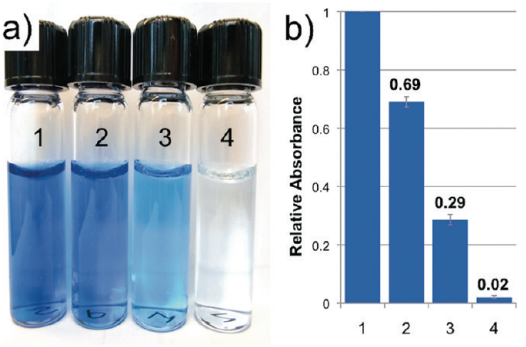

Figure 7. (a) Recovered and alkalized aqueous solutions of BTB after static adsorption for 48 h: stock (1), PMS-ir (2), MIMO-ir (3), and NIMO-ir (4); (b) relative absorbance of solutions 1 to 4 at 615 nm, with relative absorbances indicated at the top of each column.

(Figure 7a), while the solution suspended with NIMO-ir (4) is colorless. This somewhat counterintuitive result can be explained by considering the nature of the pore surfaces of each of the three materials. Surface silanol groups are present on all three species, as indicated by the Q^2 and Q^3 signals observed in ^{29}Si CP MAS NMR (Figure 2b). Additionally, NIMO-ir and MIMO-ir possess primary amine groups, with NIMO-ir having about 15% more amines per gram of material than MIMO-ir. BTB is only slightly soluble in water, so it is to be expected that it would readily be desolvated by appropriate interactions with the surface of the materials. In this case, 31% of the BTB is adsorbed from solution 2 by PMS-ir, indicating that there is some interaction but not enough to completely desolvate the dye (Figure 7b). MIMO-ir removes 71% of the dye from solution 3, slightly less than half of which can be attributed to silica interactions, indicating that only 40% of the dye is removed from solution by interactions with amine groups. In contrast, 98% of BTB is removed from the solution exposed to NIMO-ir (indicated both by the colorless solution and the very low relative absorbance in the UV−vis spectrum for this sample). On the basis of the trends observed in the SPE experiments, a more hydrophobic target molecule is better removed from aqueous solution than a less hydrophobic one; however, in a truly imprinted material, size selectivity also exists. In this case, size selectivity is confirmed by observing that even though MIMO-ir is better able to sequester appropriately sized bisphenol molecules than NIMO-ir, it does not remove a significantly larger and sterically bulkier bisphenol analogue such as BTB from solution, despite the proper arrangement of AP groups in the imprint sites. This could be partially due to the size of the molecule and partially due to the substitution at both carbons ortho to the phenols; however, since near quantitative removal of the dye is observed for NIMO-ir, the steric environment of the phenol is not too crowded for primary amines, so size selectivity is more likely. Some BTB is removed by MIMO-ir, which can be accounted for by considering

that a fraction of imprint sites are likely present at or very close to the surface of the pores and so are at least partially accessible to larger targets like BTB.

In conclusion, we have demonstrated the successful molecular imprinting of BPA into SBA-15-type mesoporous organosilica using a thermally reversible semicovalent imprinting strategy. Careful comparison of the properties of MIMO and MIMO-ir to those of NIMO/NIMO-ir and PMS/PMS-ir provides evidence of a mesoporous organosilica material with the BPAP organic bridging group buried in the pore walls. Low loading of the imprint precursor ensured the retention of the mesoporous structure after imprint removal, yet MIMO-ir still showed excellent binding of appropriate bisphenol species. An interesting study would probe the loading limit of a MIMO material that retains its pore structure after imprint removal; it it not likely that the loading could exceed 25%, but even this number could produce an excellent material. Shape selectivity was demonstrated in the poor binding of smaller phenol molecules, as was size selectivity, evinced by the poor sequestration of BTB in MIMO-ir compared to NIMO-ir; this highlights the difference in behavior of AP groups buried in the walls from AP groups located specifically on the surface of the pores. We have also observed an unexpected trend in the affinity of NIMO-ir and PMS-ir for bisphenol species of different hydrophobicity, which could be used to screen for new imprint molecules for silica.[25] An interesting study would compare materials imprinted with a range of bisphenol species of varying size and hydrophobicity and their extraction properties for different bisphenol molecules. On the basis of the affinities demonstrated in this study, a BPAF-imprinted MIMO should show the greatest binding properties with preference for BPAF. A recent report of molecular imprinting in MCM-41-type materials[15] has prompted us to examine whether a nanometer-scale change in wall thickness can result in improved or diminshed target interaction, and whether there is a lower limit to the thickness of the enclosing matrix, below which the structural integrity and thus the selectivity of the imprint site is compromised. This is of particular concern in the synthetic method described herein, as it involves a hydrothermal treatment to remove the imprint. Investigations of this are currently underway.

METHODS

Materials. (3-Isocyanatopropyl)triethoxysilane (ICPTES), tetraethyl orthosilicate (TEOS), phenol (P), resorcinol (R), 4,4′-biphenol (BP), bisphenol F (BPF), bisphenol A (BPA), hexafluorobisphenol A (BPAF), bromothymol blue (BTB), and Pluronic P123 (P123, $M_n \sim 5750$ g/mol) were purchased from Aldrich and used without further purification.

Precursor Synthesis—BPAP. In a typical batch, BPA (2.751 g, 12 mmol) and ICPTES (5.97 mL, 24 mmol) were added to 25 mL of dry tetrahydrofuran (THF) in a round-bottomed flask and allowed to react with stirring under N_2 at 65 °C for 20 h. The solvent was removed by rotary evaporator, and the resultant oily liquid was characterized by FTIR, ^{1}H NMR, and ^{13}C NMR. The yield, estimated from ^{1}H NMR, was 90%. For FTIR and NMR spectra of the precursor, see Supporting Information.

Mesoporous Material Synthesis. A stock template solution was prepared by mixing P123 (8.4 g, 1.5 mmol), NaCl (24.4 g, 0.418 mol), water (69.6 g, 3.86 mol), and 2 M HCl (208.8 g, 11.6 mol H_2O, 0.42 mol HCl) and stirring until complete dissolution was achieved.

Molecular imprinted mesoporous organosilica (MIMO) was prepared by adding a predissolved solution of BPAP (0.347 g, 0.48 mmol) in TEOS (1.8000 g, 8.6 mmol) to 44 g of stock template solution with stirring. Non-imprinted mesoporous organosilica (NIMO) was prepared by adding a predissolved solution of ICPTES (0.2365 g, 0.96 mmol) in TEOS (1.8000 g, 8.6 mmol) to 44 g of stock template solution with stirring. Periodic mesoporous silica was prepared by adding TEOS (2.000 g, 9.6 mmol) to 44 g of stock template solution with stirring. Each mixture was stirred at room temperature for 24 h, then transferred to an 80 °C oven and cured quiescently for 24 h. The resultant powders were isolated by filtration, rinsed, and then washed free of P123 by Soxhlet extraction with ethanol for 20 h. The washed powders were characterized by FTIR, ^{13}C CP MAS solid-state NMR, ^{29}Si CP MAS solid-state NMR, X-ray diffraction, nitrogen adsorption, and transmission electron microscopy.

Imprint Removal. MIMO (1 g) was suspended in dimethylsulfoxide (DMSO) in a round-bottomed flask. Several drops of distilled water were added, and the suspension was heated to 160 °C for 5 h with stirring. The imprint-removed material, MIMO-ir, was isolated by filtration, rinsed three times with alternately distilled water and ethanol, twice more with ethanol, and then oven-dried. The same treatment was carried out on NIMO (1 g) to generate NIMO-ir and PMS (1 g) to generate PMS-ir. The powders were characterized by FTIR, ^{13}C CP MAS solid-state NMR, ^{29}Si CP MAS solid-state NMR, X-ray diffraction, nitrogen adsorption, and transmission electron microscopy. MIMO-ir and NIMO-ir were also characterized by ^{29}Si HPDEC MAS solid-state NMR.

Solid-Phase Extraction and Static Adsorption Experiments. Solid-phase extraction (SPE) cartridges were prepared by packing 80 mg each of MIMO-ir, NIMO-ir, and PMS-ir into respective 3 mL polyethylene syringes between circles of extra-thick cellulose filter paper. In series 1, an aqueous stock solution of BPF (1.1×10^{-4} M), BPA (1.1×10^{-4} M), and BPAF (1.0×10^{-4} M) was prepared and analyzed by HPLC. Each SPE cartridge was loaded with 1.0 mL of stock solution, which was allowed to flow through by gravity and collected. Each cartridge was then rinsed with 1.0 mL of deionized water, which was allowed to flow through and collected. Each cartridge was then eluted with 6.0 mL of acetonitrile (ACN), which was allowed to flow through, collected, evaporated to dryness, and redissolved in 1.0 mL of ACN. Each fraction, load, rinse, and elute, respectively, was analyzed by HPLC and compared to the stock solution. In series 2, an identical solid-phase extraction procedure was used for a solution of P, R, BP, and BPA in water, with all analytes at a concentration of 1.0×10^{-4} M. All solid-phase extraction tests were done in triplicate.

Static adsorption of BTB was performed by suspending 10 mg each of MIMO-ir, NIMO-ir, and PMS-ir in 10.0 mL of an aqueous solution of BTB (approximately 2.5×10^{-5} M) and briefly sonicating each sample to fully disperse the powders. The suspensions were then allowed to stand undisturbed for 48 h. Samples of each solution were collected and alkalized with a few drops of concentrated $NaOH_{(aq)}$. The absorbance at 615 nm of each solution (corresponding to the maximum absorbance of BTB at basic pH, as well as the maximun absorbance of the alkalized stock) was taken and compared to the stock dye solution. Static adsorption was performed in triplicate.

Instrumentation. Fourier transform infrared spectroscopy was carried out on a Perkin-Elmer Spectrum BX FT-IR system. BPAP

was characterized as a liquid film on KBr windows. All powders were prepared as KBr pellets.

Solution ^{1}H and ^{13}C NMR spectra of BPAP in $CDCl_3$ were obtained on a Mercury 300 spectrometer.

All solid-state NMR experiments were carried out on a Bruker Avance 200 MHz spectrometer with powder samples packed into a 7 mm zirconia rotor and spun at a frequency of 5 kHz. ^{13}C CP MAS experiments were carried out using a 1 ms contact time, composite pulse proton decoupling and ramp cross-polarization, with an average of 3000 scans acquired per sample. ^{29}Si CP MAS experiments were carried out using a 10 ms contact time with an average of 6000 scans acquired per sample. ^{29}Si HPDEC MAS experiments were carried out using high-power decoupling with a 5 μs 90° pulse, a 30 s recycle delay, and a 5 μs prescan delay, with 1550 scans acquired per sample.

Transmission electron microscopy images were obtained on a Hitatchi H-7000 microscope with a 100 kV accelerating voltage.

Powder X-ray diffraction was carried out on a Bruker AXS NanoStar SAXS diffractometer equipped with a high-power Cu Kα source and long, 670 mm, beam path to a GADDS area detector for 2D images. A double Gobel-Mirror system was used for perfect collimation of the primary X-ray beam to a 0.35 mm spot, which passed through the sample in transmission mode. The sample's camera and the whole beam path were kept under vacuum (10^{-8} mmHg) to eliminate air-scattering and to improve the resolution. The obtained 2D image of each sample was then integrated pixel-by-pixel to convert the whole image area to a conventional $I/2\theta$ scaled plot.

Nitrogen adsorption was carried out on a Quantachrome AS1C-VP2 with a bath temperature of 77 K. All samples were outgassed for at least 16 h at 100 °C before being weighed. Surface areas were determined using Brunauer–Emmett–Teller (BET) theory, and pore size distributions were calculated using Barrett–Joyner–Halenda theory from the adsorption branch.

HPLC experiments were carried out on a Phenomenex Gemini-NX 5 μ C18 110 Å column with dimensions 150 × 4.6 mm, using a Perkin-Elmer Series 410 LC pump, a Perkin-Elmer Series 200 autosampler, a Shimadzu CTO-6A column oven, and a Shimadzu SPD-10A UV–vis detector. Sample injections of 50 μL, a flow rate of 1.0 mL/min, a column temperature of 35 °C, UV detection at 280 nm, and a mobile phase of varying ratios of acetonitrile (ACN) and aqueous 0.01 M H_3PO_4 (PA) were used. Series 1 analytes were run using isocratic elution with 50:50 ACN/PA. Series 2 analytes were run with a mixed pump program with the following eluent compositions and times: 2.5 min at 35:65 ACN/PA, 1.5 min at 80:20 ACN/PA, 6 min at 35:65 ACN/PA. Integrated peak areas for each analyte were obtained using TC4 software and normalized to the corresponding stock solution.

UV–vis spectra were obtained on a Cary 100 Bio UV–vis spectrometer in a quartz cuvette with 1 cm path length. The absorbances were normalized to that of the stock solution at its maximum absorbance (at 643 nm).

Acknowledgment. The authors acknowledge S. Petrov for his help with XRD analysis, D. Mathers for his help with HPLC method development, and I. Gourevich for assistance with TEM. G.A.O. is a Government of Canada Research Chair in Materials Chemistry and Nanochemistry. He thanks the Natural Sciences and Engineering Research Council (NSERC) of Canada for strong and sustained financial support of his research.

Supporting Information Available: Characterization of BPAP; FTIR spectra of all mesoporous materials; N_2 adsorption–desorption isotherms of all mesoporous materials. This material is available free of charge *via* the Internet at http://pubs.acs.org.

REFERENCES AND NOTES

1. Polyakov, M. V. *Zh. Fiz. Khim.* **1931,** *2*, 799–805.
2. Alexander, C.; Andersson, H.; Andersson, L.; Ansell, R.; Kirsch, N.; Nicholls, I.; O'mahony, J.; Whitcombe, M. Molecular Imprinting Science and Technology: A Survey of the Literature for the Years up to and Including 2003. *J. Mol. Recognit.* **2006,** *19*, 106–180.
3. Katz, A.; Davis, M. E. Molecular Imprinting of Bulk, Microporous Silica. *Nature* **2000,** *403*, 286–289.
4. Graham, A. L.; Carlson, C. A.; Edmiston, P. L. Development and Characterization of Molecularly Imprinted Sol–Gel Materials for the Selective Detection of DDT. *Anal. Chem.* **2002,** *74*, 458–467.
5. Ki, C. D.; Oh, C.; Oh, S. G.; Chang, J. Y. The Use of a Thermally Reversible Bond for Molecular Imprinting of Silica Spheres. *J. Am. Chem. Soc.* **2002,** *124*, 14838–14839.
6. Arsenault, A. C.; Puzzo, D. P.; Manners, I.; Ozin, G. A. Photonic-Crystal Full-Colour Displays. *Nat. Photonics* **2007,** *1*, 468–472.
7. Díaz-García, M.; Laíño, R. Molecular Imprinting in Sol–Gel Materials: Recent Developments and Applications. *Microchim. Acta* **2005,** *149*, 19–36.
8. Makote, R.; Collinson, M. M. Template Recognition in Inorganic–Organic Hybrid Films Prepared by the Sol–Gel Process. *Chem. Mater.* **1998,** *10*, 2440–2445.
9. Fireman-Shoresh, S.; Turyan, I.; Mandler, D.; Avnir, D.; Marx, S. Chiral Electrochemical Recognition by Very Thin Molecularly Imprinted Sol–Gel Films. *Langmuir* **2005,** *21*, 7842–7847.
10. Walcarius, A.; Collinson, M. M. Analytical Chemistry with Silica Sol–Gels: Traditional Routes to New Materials for Chemical Analysis. *Annu. Rev. Anal. Chem.* **2009,** *2*, 121–143 and references therein.
11. Dai, S.; Burleigh, M. C.; Shin, Y.; Morrow, C. C.; Barnes, C. E.; Xue, Z. Imprint Coating: A Novel Synthesis of Selective Functionalized Ordered Mesoporous Sorbents. *Angew. Chem., Int. Ed.* **1999,** *38*, 1235–1239.
12. Markowitz, M. A.; Kust, P. R.; Deng, G.; Schoen, P. E.; Dordick, J. S.; Clark, D. S.; Gaber, B. P. Catalytic Silica Particles *via* Template-Directed Molecular Imprinting. *Langmuir* **2000,** *16*, 1759–1765.
13. Kresge, C. T.; Leonowicz, M. E.; Roth, W. J.; Vartuli, J. C.; Beck, J. S. Ordered Mesoporous Molecular Sieves Synthesized by a Liquid-Crystal Template Mechanism. *Nature* **1992,** *359*, 710–712.
14. Zhao, D.; Feng, J.; Huo, Q.; Melosh, N.; Fredrickson, G. H.; Chmelka, B. F.; Stucky, G. D. Triblock Copolymer Syntheses of Mesoporous Silica with Periodic 50 to 300 Angstrom Pores. *Science* **1998,** *279*, 548–552.
15. Dai, S. Hierarchically Imprinted Sorbents. *Chem.—Eur. J.* **2001,** *7*, 763–768.
16. Jung, B. M.; Kim, M. S.; Kim, W. J.; Chang, J. Y. Molecularly Imprinted Mesoporous Silica Particles Showing a Rapid Kinetic Binding. *Chem. Commun.* **2010,** *46*, 3699–3701.
17. Vandenberg, L. N.; Hauser, R.; Marcus, M.; Olea, N.; Welshons, W. V. Human Exposure to Bisphenol A (BPA). *Reprod. Toxicol.* **2007,** *24*, 139–177.
18. Whitcombe, M. J.; Rodriguez, M. E.; Villar, P.; Vulfson, E. N. A New Method for the Introduction of Recognition Site Functionality into Polymers Prepared by Molecular Imprinting: Synthesis and Characterization of Polymeric Receptors for Cholesterol. *J. Am. Chem. Soc.* **1995,** *117*, 7105–7111.
19. Massiot, D.; Fayon, F.; Capron, M.; King, I.; Le Calvé, S.; Alonso, B.; Durand, J. O.; Bujoli, B.; Gan, Z.; Hoatson, G. Modelling One- and Two-Dimensional Solid-State NMR Spectra. *Magn. Reson. Chem.* **2002,** *40*, 70–76.
20. Shea, K. J.; Loy, D. A. A Mechanistic Investigation of Gelation. The Sol–Gel Polymerization of Precursors to Bridged Polysilsesquioxanes. *Acc. Chem. Res.* **2001,** *34*, 707–716.
21. Hatton, B.; Landskron, K.; Whitnall, W.; Perovic, D.; Ozin, G. A. Past, Present, and Future of Periodic Mesoporous Organosilicas—The PMOs. *Acc. Chem. Res.* **2005,** *38*, 305–312.
22. Maria Chong, A. S.; Zhao, X. S. Functionalization of SBA-15 with APTES and Characterization of Functionalized Materials. *J. Phys. Chem. B* **2003,** *107*, 12650–12657.
23. Hoffmann, F.; Cornelius, M.; Morell, J.; Fröba, M. Silica-Based Mesoporous Organic–Inorganic Hybrid Materials. *Angew. Chem., Int. Ed.* **2006,** *45*, 3216–3251.
24. Sing, K. S. W. Reporting Physisorption Data for Gas Solid Systems—With Special Reference to the Determination of

Surface-Area and Porosity. *Pure Appl. Chem.* **1982,** *54*, 2201–2218.
25. This screening concept was originally proposed for organic polymers by Claudio Baggiani of the University of Turin at the MIP2010 conference in New Orleans in August 2010, where he reported a connection between the affinity of blank polymers and their effectiveness as MIPs for given imprint molecules. Our results suggest a similar strategy would be valid for silica and possibly other inorganic species.